Optical Materials 47 (2015) 135–142

Contents lists available at ScienceDirect

Optical Materials

journal homepage: www.elsevier.com/locate/optmat

Synthesis, characterization and luminescence properties of Eu^{3+}-doped hydroxyapatite nanocrystal and the thermal treatment effects

Flávia R.O. Silva [a], Nelson B. de Lima [a], Ana Helena A. Bressiani [a], Lilia C. Courrol [b], Laércio Gomes [c,*]

[a] Centro de Ciência e Tecnologia dos Materiais, Instituto de Pesquisas Energéticas e Nucleares, IPEN-CNEN/SP, Butantã, P.O. Box 11049, São Paulo, SP 05422-970, Brazil
[b] Universidade Federal de São Paulo, Campus Diadema, SP, Brazil
[c] Centro de Lasers e Aplicações, Instituto de Pesquisas Energéticas e Nucleares, Brazil

ARTICLE INFO

Article history:
Received 6 May 2015
Received in revised form 30 June 2015
Accepted 6 July 2015
Available online 13 July 2015

Keywords:
Hydroxyapatite
Europium luminescence
Time-resolved luminescence spectroscopy
Energy transfer
Luminescence efficiency
Nanophosphors

ABSTRACT

In this work, we present the synthesis, characterization and the luminescence properties of $Ca_{10}(PO_4)_6(OH)_2$ (hydroxyapatite/HAp) nanocrystals doped with europium trivalent ions. The most important processes that lead to europium emissions in the visible region were identified. Eu:HAp nanopowder excited at 394 nm (or 460 nm) exhibits several emissions: (i) weak emissions at 579 nm, 592 nm and 616 nm due to the $^5D_0 \rightarrow {}^7F_0$, $^5D_0 \rightarrow {}^7F_1$ and $^5D_0 \rightarrow {}^7F_2$ transitions, respectively, with europium ion occupying site I in hydroxyapatite structure and (ii) strong emissions due to the $^5D_0 \rightarrow {}^7F_0$ (574 nm), $^5D_0 \rightarrow {}^7F_1$ (602 nm) and $^5D_0 \rightarrow {}^7F_2$ (610–630 nm) transitions, when Eu^{3+} is occupying site II. The emission spectrum and the time-resolved luminescence analysis showed that the HAp nanocrystals (nanopowder) thermally treated at temperature (T) between 500 and 800 °C have a change in the initial Eu^{3+} site distribution of 100 % of Eu^{3+} at site I to a more stable one where the majority of europium ions are at site II: 30% remains at site I and 70% migrates to site II. In addition, an enhancement of the Eu^{3+} emission intensity is observed due to the increasing crystallite size. A time-resolved luminescence investigation using a short pulse laser excitation at 460 nm was employed to measure the luminescence decays and to determine the most important mechanisms involved in the deexcitation process of $^5D_0$ excited state of Eu^{3+}, where it is seen a fast (2.9 μs) energy transfer from Eu^{3+}- site I (donor) to Eu^{3+}- site II (acceptor) in the thermally treated nanopowders with $T > 500$ °C. The initial presence of 100% of Eu^{3+} at site I in the synthesized nanocrystals is gradually modified by the thermal treatments with temperatures above 500 °C by thermal activation of Ca^{2+} vacancy (the charge compensator) diffusion through the HAp lattice, which propitiates the Ca^{2+}- vacancies and Eu^{3+} ions to exchange positions in the lattice. By this thermal activated mechanism, Eu^{3+} ion migrates through the lattice until get the final distribution of 30% at site I and 70% at site II. As a result, the complete description of the Eu^{3+} ($^5D_0$) decay and the energy transfer process from Eu^{3+} (site I) → Eu^{3+} (site II) were proposed.

1. Introduction

With the oncoming of the nanoscience and nanotechnology in the past few decades, this new field has exerted great impact on nanophosphor biomaterials, then studies on the synthesis and properties of nanophosphors [1] have received intense research interest due to their application as luminescent labels in bioimaging, and as donors in energy transfer systems [2,3]. In particular, $Ca_{10}(PO_4)_6(OH)_2$ (hydroxyapatite/HAp) crystal, which is the mineral constituent (30–70%) of bones and teethes, has received attention for its biocompatibility and osteoconductivity.

Hydroxyapatites are chemical compounds of calcium phosphates of special interest in medicine, since they are the major component of all mammalian calcified tissues [4]. The synthetic hydroxyapatite has the advantage of being doped with a variety of cation ions that can change the bioceramic's characteristics to a specific application. HAp nanoparticles are considered as biocompatible and biodegradable carriers of drug, bioactive bone repairs and as coatings for metallic prostheses to improve their biological properties [5]. HAp crystallizes in the hexagonal structure ($P6_3/m$) with a lattice parameter $a = b = 9.42$ Å and $c = 6.88$ Å.

Luminescent HAp can be achieved replacing the calcium ion in the crystal lattice by rare earth ions. Fluorescent labeling can realize the continuous and nondestructive observations, which is helpful for monitoring the implanted subject [6], the delivering progression of drug carriers [7], etc. In particular, HAp can be used

* Corresponding author.
E-mail address: lgomes@ipen.br (L. Gomes).

http://dx.doi.org/10.1016/j.optmat.2015.07.006
0925-3467/

as luminescent materials when activated by Eu^{3+} ions in substitution of Ca^{2+} ions in non-center-symmetrical and non-equivalent sites, (I) and (II), where Ca^{2+} (I) is surrounded by nine oxygen ions and Ca^{2+} (II), coordinated by six oxygen ions and the hydroxyl group with their relative abundances being in the ratio 4:6 [8]

Trivalent europium ion has a $4f^6$ configuration leading to an intense orange-red emission around 590–625 nm, due to various $^5D_0 \rightarrow {}^7F_{0\text{-}4}$, especially $^5D_0 \rightarrow {}^7F_1$ and $^5D_0 \rightarrow {}^7F_2$ transitions. Europium fluorescence in hydroxyapatite is reported to depends on calcium site occupied: when Eu^{3+} substitutes Ca^{2+} (I), the emission is observed at 590–600 nm, corresponding to $^5D_0 \rightarrow {}^7F_1$ transition, 610–625 nm to $^5D_0 \rightarrow {}^7F_2$, 650–660 nm to $^5D_0 \rightarrow {}^7F_3$ and 689–710 nm to $^5D_0 \rightarrow {}^7F_4$, and when Ca^{2+} (II) is the substituted site, the europium transitions observed are $^5D_0 \rightarrow {}^7F_0$, at 570–580 nm, $^5D_0 \rightarrow {}^7F_1$ at 600–608 nm, and $^5D_0 \rightarrow {}^7F_2$ at 615–631 nm [9–13]. These typical characteristics in each calcium site enable one to ascertain the europium site in the HAp. It has been mentioned that the method of HAp synthesis [14,15] and the Eu^{3+} concentration can influence the site occupation [16–18], but the influence of the temperatures of the thermal treatments is not yet clear.

Herein, the Eu^{3+} ions doped HAp (Eu:HAp) nanoparticles were synthesized by co-precipitation method (crystallite size ~23 nm). The effects of thermal treatments' temperature on luminescent properties, lifetime, phase composition, crystal size and crystallinity of Eu:HAp were analyzed in order to investigate the fluorescence emission of the two sites of Eu^{3+} in HAp.

The multiple processes of energy transfers that occur when this material is excited near 460 nm were investigated. The luminescence transients at 574 and 590 nm of $^5D_0$ excited state of Eu^{3+} were measured for Eu:HAp nanocrystals induced by pulsed laser excitation at 460 nm. The luminescence efficiency of $^5D_0$ excited state and its dependence on the thermal treatment temperature and mean crystallite size were determined.

2. Experimental procedure

The nanopowders were obtained by the co-precipitation method, wherein the phosphoric acid (H_3PO_4, Synth – Brazil) diluted in deionized water (0.3 M) is slowly added drop by drop (8 ml/min rate) into a suspension of calcium hydroxide ($Ca(OH)_2$, Synth- Brazil) and europium nitrate ($EuNO_3.5H_2O$, Sigma Aldrich)(0.5 M) vigorously stirring to form: $Ca_{8.6}Eu_{1.4}(PO_4)_6(OH)_2$. The pH value was adjusted to 10 using ammonia solution.

The synthesis of pure hydroxyapatite (HAp) was performed following the same procedure for Eu:HAp synthesis. After the addition of the phosphoric acid a white precipitate was formed, and the resulted solution was maintained at room temperature for 24 h. Then, the solutions (HAp and Eu:HAp) were filtrated and washed with deionized water. The powders were dried at 60 °C for 24 h.

The dried powders were heated at T = 500 °C and 600 °C for 1 h and T = 800 °C, 1000 °C and 1200 °C for 3 h. Samples were characterized by X-ray diffraction (XRD) using a Multiflex Rigaku diffractometer using the Cu kα (λ = 0.1542 nm) radiation. The crystallite size was determined by Scherrer's formula and the (002) X-ray diffraction peak was used. The nanopowders were dispersed in absolute isopropanol and ultrasound treated to avoid particles agglomeration, and then were dropped on a copper grid to be observed by transmission electronic microscopy (JEM 2010 – JEOL). To Field Emission Gun scanning electron microscopy (FEG JSM 6701F – JEOL) analysis the samples were carbon-coated.

Fluorescence spectroscopy was carried out, at room temperature, in a Fluorolog 3 Fluorimeter from Jobin Yvon that uses an optical bundle to excite and collecting the luminescence signals for analyze.

The luminescence lifetime measurements were performed at room temperature, where the samples were excited by pulsed laser radiation generated by a tunable OPO-VIS pumped (Rainbow from OPOTEK, USA) by the third harmonic of a Q-switched Nd:YAG (yttrium aluminum garnet) laser (Brilliant B from Quantel, France). Laser pulse widths of 4 ns at 460 nm were used to directly excite the $^5D_0$ excited state of Eu^{3+}. The nanopowder was accomplished in a sample holder with a CaF_2 window allowing the absorption (diffuse reflection) and luminescence measurements by collecting the frontal emission using an optical fiber bundle of 2 mm diameter. Luminescence signals were analyzed by the 0.25 m Kratos monochromator and detected by the EMI S-20 photomultiplier tube EMI (response time of 10 ns). Luminescence lifetime was measured using a digital oscilloscope of 100 MS s^{-1} model TDS 410 from TEKTRONIX interfaced to a microcomputer.

3. Results

The synthesized nanopowders have shown the hexagonal phase of $Ca_{10}(PO_4)_6(OH)_2$ corresponding to the ICDD file n°. 9–432, however with the diffraction profile broadening, due to the small mean crystallite size, as seen in Fig. 1. Nevertheless, X-ray diffraction peaks become narrow after thermal treatment at T > 600 °C due to the crystallite growth and increasing of crystallinity (Fig. 1). The synthesized mean crystallite size (d) is small (23 nm) and shows no great variation until the treatment at 600 °C (26 nm). The changes in the mean crystallite sizes after heating the samples at various temperatures are given as follows: d = 24.3 nm (500 °C); d = 26.3 nm (600 °C); d = 56.6 nm (800 °C); d = 177.1 nm (1000 °C) and d = 232.8 nm (1200 °C).

The mean crystallite size for undoped HAp as-synthesized is 27 nm and after heated at 1200 °C it reached d = 163 nm. It is possible to see in the X-ray diffraction pattern of the Eu:HAp treated at 1200 °C samples, shown in Fig. 1, the presence of a secondary phase with low concentration identified as $Ca_{2.81}Mg_{0.19}(PO_4)_2$, according to ICDD-PDF 70–682 card.

Despite the small mean crystallite size obtained after synthesis, both HAp and Eu:HAp have well-defined crystalline phase. This can be seen in the transmission micrographs shown in Fig. 2, where (A) and (B) are for HAp and (C) and (D) for Eu:HAp, both without thermal treatment samples (as-synthesized). Fig. 2(E) and (F) shown the Eu:HAp thermally treated samples at 600 °C and 800 °C, respectively. The micrographs obtained by scanning electron

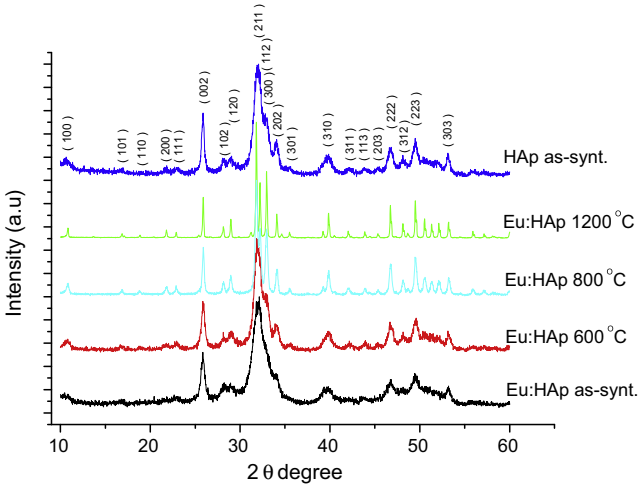

Fig. 1. X-ray diffraction pattern of hydroxyapatite pure and dopped with europium ion synthesized nanopowder before (as-synthesized) and after thermal treatment (T = 600, 800 and 1200 °C). The Miller indices of X-ray pattern were added.

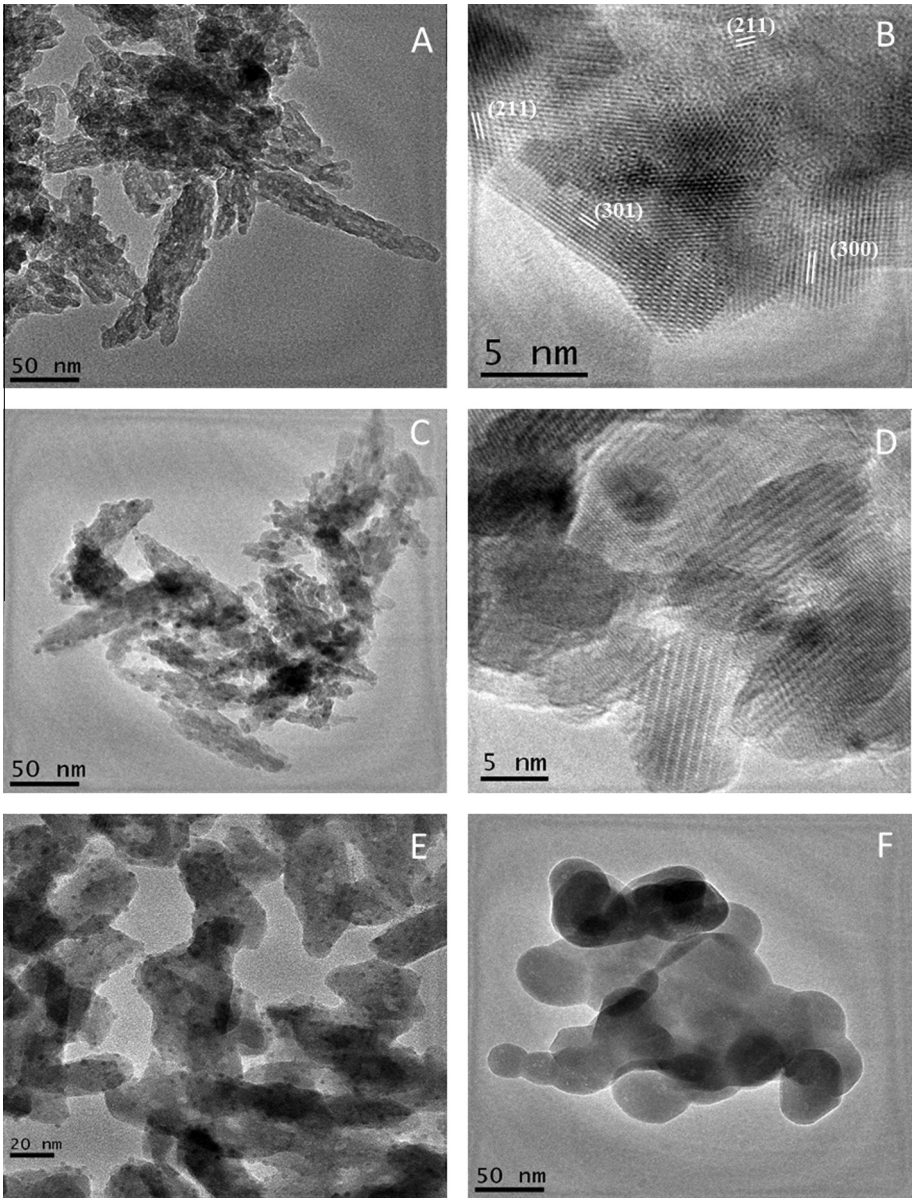

Fig. 2. TEM micrographies obtained for nanopowders HAp as-synthesized (A and B) and Eu:HAp as synthesized (C and D) and for Eu:HAp after thermal treatment at T = 600 °C (E) and T = 800 °C (F). In addition, the HRTEM image also provide the (2 1 1), (3 0 0) and (3 0 1) lattice planes of hexagonal HAp struture (B).

microscopy of HAp and Eu:HAp after thermal treatment at 1200 °C are shown in Fig. 3(A) and (B), respectively. Both presents an initial sintering and the grain growth processes. The EDS analyses confirm the presence of calcium, phosphor and europium. Spot EDS analysis showed that the small grains seen in Fig. 3(B), also presents magnesium that is an impurity of calcium hydroxide $(CaOH)_2$, as it has been identified as a secondary phase by X-ray diffraction.

Optimal emission efficiency of Eu^{3+} was observed for doping HAp nanocrystals with Eu^{3+} concentration of 1.4 mol%. In this case, the samples exhibited good luminescence signals allowing to measure the emission spectrum with fine resolution of 0.5 nm and to use the time-resolved luminescence spectroscopy to investigate the decay behavior of Eu^{3+} ($^5D_0$) excited state in the as-synthesized and thermally treated nanocrystals, besides avoiding the quenching effect at higher europium concentrations.

Emission spectra of Eu:HAp nanocrystal have several emission bands in the visible due to the $^5D_0 \rightarrow {}^7F_{0-4}$ transitions, revealing the presence of crystallographic inequivalent occupation sites. Fig. 4(a) shows that Eu^{3+} ion in the as-synthesized sample presents two main broad emission bands centered at 592 nm and 616 nm corresponding to the typical $^5D_0 \rightarrow {}^7F_1$ and $^5D_0 \rightarrow {}^7F_2$ transitions, respectively, and a weak narrow band at 579 nm, corresponding to $^5D_0 \rightarrow {}^7F_0$ transition, under 394 nm excitation wavelength. This characteristic emission spectrum is consistent with europium ion occupying Ca^{2+} (I) site [9–13,19]. The temperature increasing of the thermal treatments modifies the europium emission spectra, i.e., at T = 500 °C, the specimen emission remains weak, but it starts appearing a slight shoulder around 628 nm and two new peaks at 574 and 577 nm, correspondent to $^5D_0 \rightarrow {}^7F_0$ transition. This non-degenerate transition ($^5D_0 \rightarrow {}^7F_0$) is particularly informative about the number of lanthanide occupation sites in luminescent materials [19]. The presence of only one $^5D_0 \rightarrow {}^7F_0$ transition in the as-synthesized sample measured indicates a unique europium site occupancy that is the Ca^{2+} (I) site. The presence of two new peaks at 574 and 577 nm observed after the thermal treatment

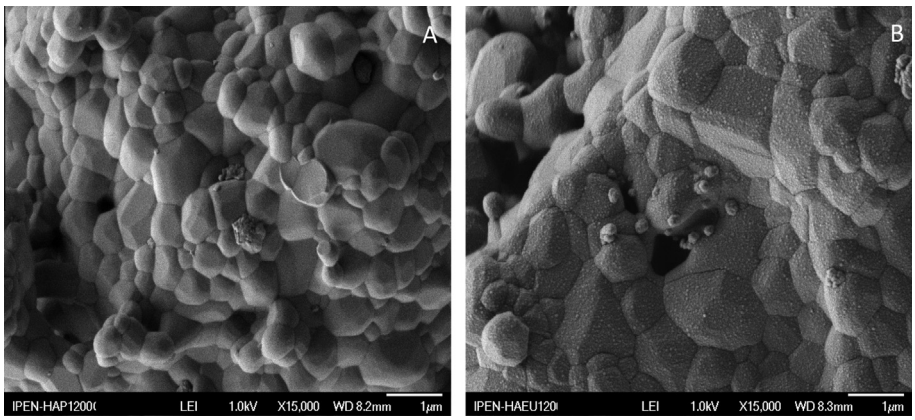

Fig. 3. FEG micrographies obtained for samples thermally treated at 1200 °C for (a) HAp and (b) Eu:HAp.

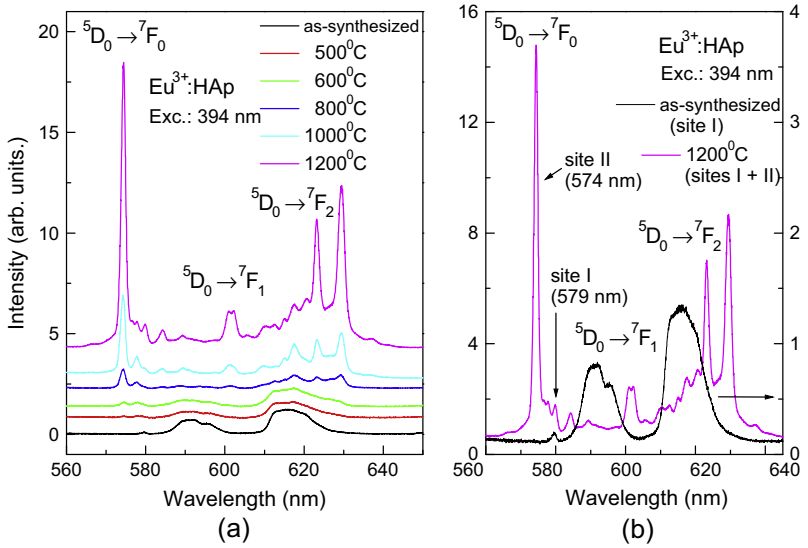

Fig. 4. (a) Emission spectra of Eu:HAp samples as-synthesized nanopowder and after thermal treatments at 500, 600, 800, 1000 and 1200 °C using monochromatic light excitation at 394 nm. (b) shows the emission spectra measured for the samples as-synthesized and for the thermally treated one at $T = 1200$ °C for comparison.

at 500 °C, is an indicative of the presence Eu^{3+} in two new sites of symmetry [12,19]. These new sites are a consequence of the initial migration of Eu^{3+} from Ca^{2+} (I) to Ca^{2+} (II) by a diffusion process.

The emission spectrum of samples calcined at 600 °C is similar of that treated at 500 °C. At 800 °C, the fluorescence spectrum is significantly distinguished from those at lower temperature as shown in Fig. 4(a). At this point, the complete migration of Eu^{3+} ions is probably achieved, which means that most of europium ions is located at Ca^{2+} (II) site [33,19]. In this case, the $^5D_0 \rightarrow {}^7F_2$ emission splits in two sharper peaks at 623.2 and 629.5 nm, and the emission of Eu:HAp is composed of almost equal contributions from $^5D_0 \rightarrow {}^7F_0$ and $^5D_0$ – $^7F_2$ transitions, which gives rise to an orange-red emission. Until 600 °C, the two new lines at 574 and 577 nm, from $^5D_0 \rightarrow {}^7F_0$ transition, present same intensity contributions, but at 800 °C, the 574 nm line starts to be more intense than the 577 and 579 nm line, and this difference will be bigger as the thermal treatment temperature increases. After the thermal treatment at $T = 1000$ °C, the $^5D_0 \rightarrow {}^7F_0$ transition of Eu^{3+} in the Ca^{2+} (II) site becomes the strongest and narrower emission band of the sample with maximum at 574 nm – see Fig. 4(a). Fig. 4(b) evidences the emission spectra differences between the as-synthesized sample and the thermally treated one at 1200 °C as described above.

The excitation wavelength at 460 nm is better at promoting the higher Eu^{3+} emission intensity when the ion is located at site II or Ca^{2+} (II). The emission at 590 nm and 574 nm were choose for representing the characteristic emission from Eu^{3+} (I) and Eu^{3+} (II) centers, respectively, considering that the emission spectra of both centers have minimum emission superposition at these choose wavelengths, to measure the luminescence decays and to determine the most important mechanisms (electronic processes) involved in the de-excitation process of Eu^{3+} in Ca^{2+} (I) and Ca^{2+} (II) sites by using the time-resolved luminescence spectroscopy technique.

The luminescence kinetic of an acceptor state that is indirectly excited by the donor–acceptor (or D–A) energy transfer is given by Eq. (1), which has been derived elsewhere [19] for an energy transfer that includes Burshtein (or Inokuti–Hirayama, where $\omega = 0$) model for the donor decay due to a dipole–dipole interaction – Eq. (2) [20].

$$I(t) = I_0 \exp\left(-\frac{t}{\tau_d} - \omega t - \gamma\sqrt{t}\right) \quad (1)$$

$$I(t) = I_0\left\{\exp\left(-\frac{t}{\tau_A}\right) - \exp\left(-\frac{t}{\tau_d} - \omega t - \gamma\sqrt{t}\right)\right\}, \quad (2)$$

where τ_A is the luminescence lifetime of the acceptor (A) excited state and τ_d is the intrinsic lifetime of the donor (D) excited ion. γ is the energy transfer parameter (given in $s^{-1/2}$) due to the donor to acceptor direct transfer and ω is the energy transfer parameter (given in s^{-1}) due to the migration contribution through donor excited level. The first term of Eq. (2) gives the luminescence decay of the acceptor and the second gives the luminescence risetime, which should be equal to the donor total lifetime. The risetime constant (or the donor decay constant) was obtained by integration according to Eq. (3) for the case of a non-exponential process.

$$\tau = \int_0^\infty \exp\left(-\frac{t}{\tau_d} - \omega t - \gamma\sqrt{t}\right)dt. \quad (3)$$

For instance, if the diffusion process between donor states dominates the energy transfer mechanism (or $\omega >> \gamma^2$) the donor decay will be exponential and the acceptor risetime will be exponential. We have identified two types of equations to describe the luminescence kinetics of Eu^{3+} centers in HAp, where Eq. (4) was used to fit the decay of $^5D_0$ excited level of Eu^{3+} (site I) centers (590 nm emission) and Eq. (5) was employed to fit the luminescence kinetic of the Eu^{3+} (site II) centers, which also works as acceptors centers (574 nm emission). Eqs. (4) and (5) have been used to describe the luminescence kinetic involving energy transfer elsewhere [21–24].

$$I_1(t) = A_1\exp\left(-\gamma_{12}\sqrt{t} - t/t_{12}\right) + B_1\exp(-\gamma_1\sqrt{t} - t/t_1) - C\exp(-t/t_{21}), \quad (4)$$

$$I_2(t) = A_2\exp(-\gamma_2\sqrt{t} - t/t_2) + B_2[\exp(-\gamma_2\sqrt{t} - t/t_2) - \exp(-t/t_{12})]. \quad (5)$$

Eqs. (4) and (5) were used to fit the 590 nm and 574 nm emissions transients of Eu^{3+} in HAp after pulsed laser excitation at 460 nm. The fitting parameters γ_{12} and t_{12} are used for describing the Eu^{3+} (site I) decay induced by Eu^{3+} (site I) → Eu^{3+} (site II) energy transfer process. γ_1 and t_1 are the parameters describing the luminescence of Eu^{3+} (site I) center remaining in the $^5D_0$ level (long decay) and t_{21} is the time constant of the Eu^{3+} (site II) → Eu^{3+} (site I) back-transfer. γ_2 and t_2 are the parameters describing the Eu^{3+} (site II) decay and t_{12} is the luminescence risetime (time constant) due to the Eu^{3+} (site I) → Eu^{3+} (site II) transfer involving the $^5D_0$ excited level of Eu^{3+} (site I) center and the $^7F_0$ ground state of Eu^{3+} (site II) center. Parameters A_1, B_1 and C are amplitudes (intensities) at $t = 0$. The calculated fraction $100 \times \frac{A_1 - C}{A_1 + B_1 - C}$ gives the contribution (%) of Eu^{3+} (I) → Eu^{3+} (II) transfer in respect to the total decay – amplitude C is related to the back-transfer process.

Experimental values of these ratios are given in Table 1. Fig. 5(a) and (b) show the luminescence decay of Eu^{3+} (site I) measured at 590 nm for Eu:HAp nanopowder as- synthesized and after thermal treatments at 500, 600, 800, 1000 and 1200 °C using a pulsed laser excitation at 460 nm with 4 ns having an average energy of 8 mJ and 10 Hz of repetition rate . Best fit of 590 nm luminescence was performed using Eq. (4) from where best fitting parameters γ_1, γ_2, γ_{12}, t_1, t_{12} and t_{21} were derived using a least squares fit – best fittings values are given in Table 1. The 590 nm emission decay measured for the nanopowder (as-synthesized) and after T = 500 °C and 600 °C exhibit an exponential decay about 550 μs, which is attributed to the presence of Eu^{3+} (site I) centers only – see Fig. 5(b). However, the emission decay (590 nm) shows a fast decay component (94%) with a time constant of 2.5 μs for nanopowder thermally treated at $T \geqslant 600$ °C, which is attributed to the Eu^{3+} (site I) → Eu^{3+} (site II). This transfer process evidences that Eu^{3+} (site II) centers are formed at expenses of Eu^{3+} (site I) centers induced by thermal treatment at $T > 600$ °C. The long decay at 590 nm luminescence (residual emission) seen in Fig. 5(b–d) having parameters γ_1 and t_1 that contributes with 5.6% of the total decay, which includes the back-transfer.

Fig. 6(a) and (b) show the luminescence kinetic of Eu^{3+} (site II) centers measured at 574 nm after pulsed laser excitation at 460 nm with 4 ns having an average energy of 8 mJ and 10 Hz. There is no luminescence for the as-synthesized Eu:HAp nanopowder, at 574 nm. Emission decay at 574 nm is observed to be non-exponential for nanopowder thermally treated at 500 °C with a time constant of 526 μs. The existence of two rising times is observed after thermal treatments at T ⩾ 600 °C: one follows the laser pulse duration (20 ns) having amplitude A_2 and another risetime with a time constant of approximately 2.5 μs and amplitude B_2, which is consistent with the Eu^{3+} (site I) → Eu^{3+} (site II) transfer previously observed at the 590 nm emission decay. A long emission decay component (574 nm) with a time constant of 671 μs (T = 1200 °C) is observed that is attributed to the intrinsic decay of Eu^{3+} (site II) centers – see Fig. 6(b). The calculated fraction $100 \times \frac{B_2}{0.94(A_2 + B_2)}$ gives the contribution (%) of Eu^{3+} (site I) → Eu^{3+} (site II) transfer in respect to the total emission (574 nm) transient, which is equal to 30% for the samples after T = 1200 °C – experimental values of these ratios are given in Table 2. Considering these results, we can estimate that the Eu^{3+} ions distribution are 30% in the Ca^{2+} (I) site and 70% in Ca^{2+} (II) site for nanopowder thermally treated at T = 1200 °C.

Fig. 7 represents an energy levels diagram proposed for Eu^{3+} in HAp nanocrystal that shows the energy transfer from Eu^{3+} (site I) to Eu^{3+} (site II) and the back-transfer processes observed according to the luminescence decay measurements.

Fig. 8 shows the Eu^{3+} ($^5D_0$) emission intensity integrated area using the emission spectrum from 560 nm to 650 nm (that includes Eu^{3+} emission from sites I and II) as a function of the mean crystallite volume (or d^3) measured for the Eu:HAp nanopowder, where d was observed to increase with the thermal treatment temperature increasing from T = 60 °C (as-synthesized and dried) to 1200 °C. Until the thermal treatment at 600 °C, the samples heated show small changes in emission intensity and crystallite volume

Table 1
Best fitting parameters of $^5D_0$ emission decay (590 nm) for the nanopowder (Eu:HAp) as grown (25 °C) and after several thermal treatments with T = 60, 500, 600, 800, 1000 and 1200 °C. t_{12} is the time constant of the Eu^{3+} (site I) → Eu^{3+} (site II) energy transfer, t_1 is the exponential component of decay of Eu^{3+} (site I) and γ_1 ($s^{-1/2}$) is the transfer parameter that does not includes excitation migration. t_{21} is the time constant of the Eu^{3+} (site II) → Eu^{3+} (site I) back-transfer process. A_1, B_1 and C are the amplitudes at $t = 0$, where A_1 is related to the energy transfer process and B_1 is due to the Eu^{3+} (site I) emission not involved in the transfer (parameters t_1 and γ_1) and C is due to the back-transfer process. The fraction of Eu^{3+} (site I) → Eu^{3+} (site II) transfer was calculated using the relation $f_{transfer} = \frac{(A_1 - C)}{(A_1 + B_1 - C)}$.

Thermal treatment	A_1 ($f_{transfer}$)	B_1 ($1-f_{transfer}$)	C	t_{12} (μs)	t_1 (μs)	γ_1 ($s^{-1/2}$)	t_{21} (μs)	R^2
Time constants of luminescence kinetic processes (590 nm) (experimental)								
60 °C	–	105	–	–	548	0	–	0.9821
500 °C	–	76	–	–	546	0	–	0.9816
600 °C	–	129	–	–	1310 (598)*	27.4	–	0.9784
800 °C	25,298 (*0.948*)	1276 (*0.052*)	615	3.0	552	0	42.75	0.9997
1000 °C	108,107 (*0.941*)	5754.4 (*0.059*)	3140	2.5	480	0.4	41.06	0.9990
1200 °C	228,687 (*0.941*)	13,687 (*0.059*)	9441	2.9	303	0	47.16	0.9982

* Integrated values using Eq. (3).

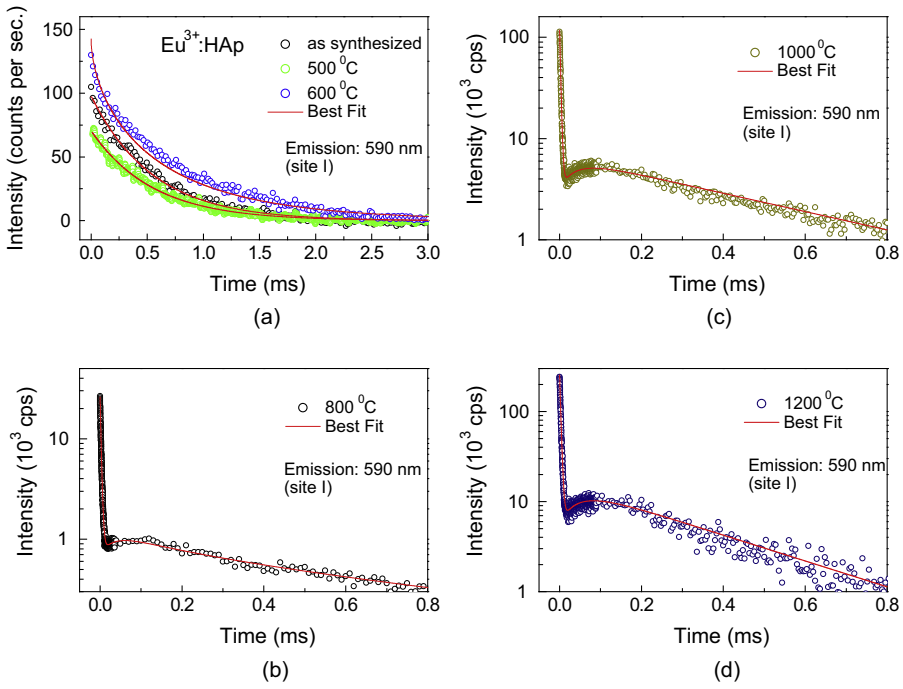

Fig. 5. Luminescence decay of $^5D_0$ excited level of Eu^{3+} (I) measured at 590 nm before (as-synthesized) and after thermal treatments at T = 500, 600, 800, 1000 and 1200 °C for Eu(1.4 mol%): HAp nanopowder using pulsed laser excitation at 460 nm (E = 8 mJ, 4 ns, 10 Hz). Best fit of luminescence transient was done using Eq. (4), which represent three mechanisms of decay: (i) fast partial decay (τ = 2.9 μs) due to the D → A energy-transfer (amplitude A_1) seen in (b–d); (ii) decay of excited Eu^{3+} (I) centers (amplitude B_1) and (iii) A → D back-transfer (amplitude C). The emission intensity of (b–d) are given in logarithmic scale.

(d^3). After thermal treatment at 800 °C, d is still in the nanosized scale (56.6 nm), but although the emission spectrum features is completed distinguished from those samples heated at 600 °C, due to the Eu^{3+} migration from site I to site II, the integrated emission intensity (area) remains approximately the same. At 1200 °C, the emission intensity is significantly higher, what can be explained based on the fact that the excitation light is being scattered in all directions and typical crystallite absorption in this case will be the summation of all photon directions ($\vec{R}$), so producing absorption of excitation light depending on the crystallite volume. At this temperature (1200 °C) the mean crystallite size reaches the highest measured value (233 nm) and the grain size increases to about micron.

4. Discussion

In fact, we have found that 100% of Eu^{3+} ions in Eu:HAp nanocrystals synthesized by co-precipitation method at room temperature and dried in the air at 60 °C for 24 h, is substituting Ca^{2+} in the Ca^{2+} (I) position (or site I) of hydroxyapatite. This fact indicates that the fast crystal growth imposed by the kinetic process makes available preferably the Ca^{2+} (I) position for Eu^{3+} occupancy, which one has the greater cationic site dimension [25], in HAp lattice, and it probably propitiates the Ca^{2+}-vacancies creation for the charge compensation mechanism. Thereby, Ca^{2+} -vacancy-Eu^{3+} can easily migrates through Ca^{2+} (I) column parallel to c-axis, by thermal activation process at higher temperatures, allowing the Eu^{3+} (site I) diffuse through the HAp lattice, until get the Ca^{2+} (II) site.

In the literature [6, 26–28] it is shown that europium-doped hydroxyapatite synthesized at low temperature exhibits an emission spectrum attributed for Ca^{2+} (I) substitution similar to those we have seen in the present work. A similar emission spectrum of Eu^{3+} ions predominately in Ca^{2+} (II) site, as we are showing, was obtained for samples prepared by combustion synthesis [13], ionic implantation [30], and samples heated at higher temperatures [29].

Our results have shown that with the thermal treatment above 500 °C, the Ca^{2+} vacancies migrate through the lattice allowing Eu^{3+} ions to exchange substitution positions, i.e., the initial Eu^{3+} distribution changed from 100% of Eu^{3+} located at Ca^{2+} (I) site in the synthesized nanocrystal (as-synthesized) to a final distribution having 30% Eu^{3+} at Ca^{2+} (I) site and 70% Eu^{3+} at Ca^{2+} (II) site after the thermal treatment at T = 800 °C. From 800 °C to 1200 °C the ratio of Eu^{3+} at Ca^{2+} (I) and Ca^{2+} (II) remains the same. It is consistent with Martin et al' results [30] that found about 80% of implanted europium ions located in Ca^{2+} (II) sites after thermal treatment at T = 500 °C. Martin et al. [30] has studied the diffusion process in natural and synthetic apatites showing that after the ionic implantation of europium, the majority of Eu^{3+} ion is partial fixed inside the apatite lattice by substitution of Ca^{2+} in Ca^{2+} (I) position, and when sufficient thermal energy is providing, as a function of time (several hours), the implanted Eu^{3+} ions can diffuse through the lattice ending the process in the position of Ca^{2+} (II) sites.

In the present work, with the Eu-redistribution, the Eu^{3+} ($^5D_0$) (site I) → Eu^{3+} ($^7F_0$) (site II) energy transfer (electronic process) takes place showing that 94% of Eu^{3+} (site I) centers can transfer its excitation to Eu^{3+} (site II), so exhibiting a short decay component of 2.5 μs – see Table 1. The long luminescence decay of Eu^{3+} (site I) (residual emission) contributes with 5% of the total decay that includes the back-transfer. The back-transfer process could be related to the peak at 577 nm, whose origin is not clear, representing a Ca^{2+} site modified by the thermal effects. Other authors, as Ternane et al. [12] and Gaft et al. [9] also identified three sites in apatites, and they have suggested the third one was related to Ca^{2+} (II) site.

In addition, the $^5D_0$ – ^7F_j transitions for each site presents its own particular characteristics, allowing the distinction between them. The emission peak position and the emission intensity of the transitions between different J levels also depend on the local symmetry of the europium ion occupancy in the nanocrystal

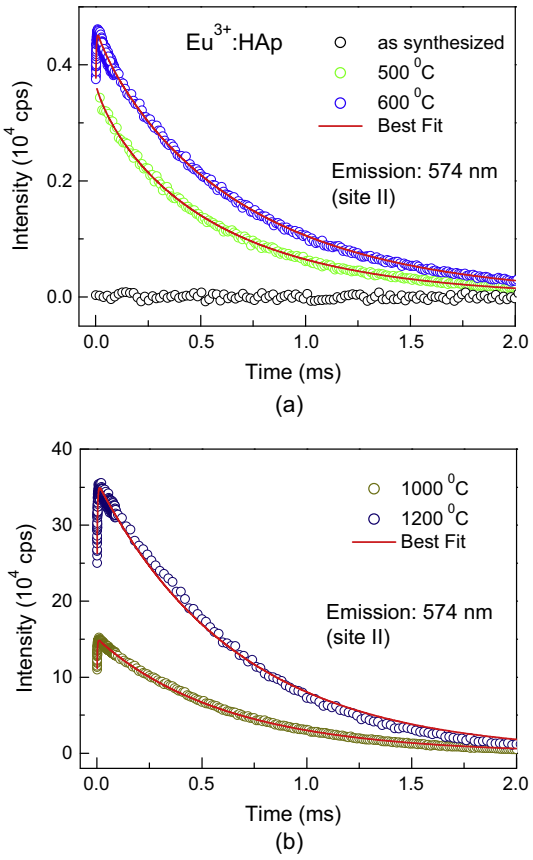

Fig. 6. Luminescence kinetic of Eu^{3+} (site II) ions measured at 574 nm before (as synthesized) and after thermal treatments at T = 500, 600, 800, 1000 and 1200 °C for Eu(1.4 mol%):HAp nanopowder using pulsed laser excitation at 460 nm (E = 8 mJ, 4 ns, 10 Hz). Best fit of luminescence transient was done using Eq. (5). Risetime of 2.9 μs is due to the Eu^{3+} (site I) → Eu^{3+} (site II) energy transfer. One must to note that the amplitudes used in Eq. (5) are related to two different mechanisms of Eu^{3+} excitation (site II): (i) direct laser excitation at 460 nm (amplitude A_2) and (ii) D → A energy-transfer (amplitude B_2).

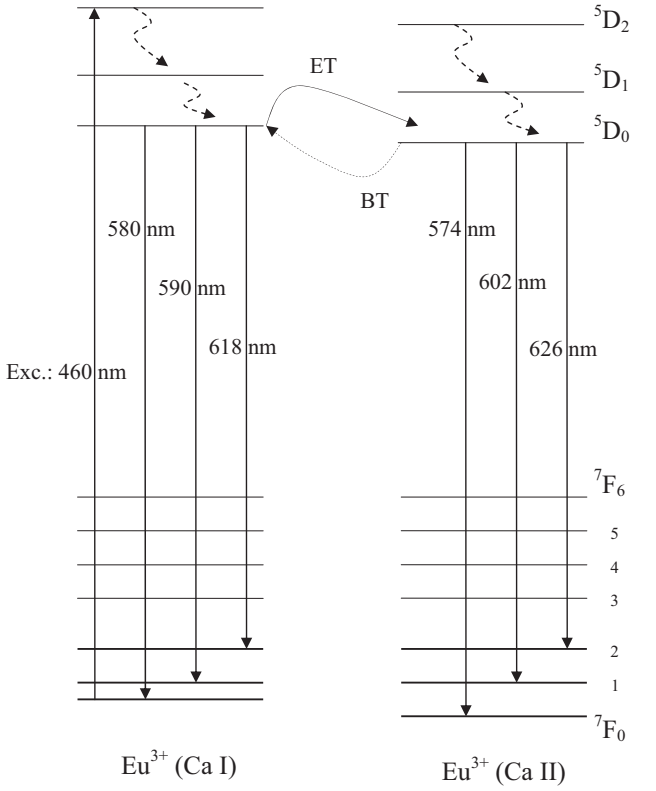

Fig. 7. Energy levels diagram proposed for Eu^{3+} in HAp nanocrystal that shows the energy transfer (ET) from Eu^{3+} (site I) to Eu^{3+} (site II) and the back-transfer (BT) processes observed according to the luminescence decay measurements. E is used to design the pulsed laser excitation at 460 nm (4 ns, 10 Hz). The emissions from Eu^{3+} at Ca^{2+} (I) site are A = 579 nm, B = 592 nm and C = 616 nm and the emissions from Eu^{3+} at Ca^{2+} (II) site are A = 574 nm, B = 602 nm and C = 623.2 and 629.5 nm (the emission wavelength was taken at the centroid position of the multiplet emission).

[31]. The crystal environment perturbs the ion vicinity and the forbidden transitions in a free ion by the parity rules of electric dipole transitions, according to Judd–Ofelt theory [32,33], become allowed as a consequence of the J-mixing states of different parity from the host matrix. Magnetic dipole transitions ($^5D_0$ – $^7F_1$) may occur only between states of the same parity. Unlike the electric dipole transitions ($^5D_0$ – $^7F_2$), the magnetic dipole transitions should not be as sensitive to the surroundings of the ion, and may be used as a standard for comparison of other transition strengths [33,34].

The relative intensity of electric dipole transition and magnetic dipole transition depends strongly on the local symmetry of europium ions sites occupancy [31]. The large ratio of the fluorescence intensities for the transitions implies a low symmetry field at the europium site [33]. In comparison with Eu^{3+} ion in Ca^{2+} (II) site, Eu^{3+} ions at Ca^{2+} (I) site have a relatively lower intensity ratio of $^5D_0$ – $^7F_2$ to $^5D_0$ – $^7F_1$.

The intensity of $^5D_0$ – $^7F_0$ transition at 574 nm is the strongest emission line when the majority of europium ion is located at Ca^{2+} (II) site, see Fig. 4. This effect probably is due to the OH^- environmental, whose electric dipole is aligned to the c-axis and is closest to Eu^{3+} ion at the Ca^{2+} (II) site. As a consequence, the strongest dipole field nearby Eu^{3+} (site II) should increase the J-mixing states of $4f^N$ and $4f^{N-1}5d$ configurations, so increasing the oscillator strength of an electric dipole transitions, i.e., the weak $^5D_0$ – $^7F_0$ emission of Eu^{3+} at site I becomes much stronger at site II.

Table 2
Best fitting parameters of $^5D_0$ emission transient (574 nm) for the nanopowder (Eu:HAp) as grown (25 °C) and after several thermal treatments with T = 60, 500, 600, 800, 1000 and 1200 °C. t_2 is the exponential component of decay (site II) and γ_2 ($s^{-1/2}$) is the transfer parameter that does not includes excitation migration. τ_2 is the luminescence lifetime (Eu^{3+} (site II)) calculated using Eq. (3). A_2 and B_2 are the amplitudes at t = 0, where B_2 is due to the Eu^{3+} (I) → Eu^{3+} (II) energy transfer. The fraction of Eu^{3+} in site I was calculated using the relation, $f = \frac{B_2}{0.94\times(A_2+B_2)}$, where 0.94 means that 94% of excited Eu^{3+} (site I) ions have transferred its excitation to Eu^{3+} (site II) centers.

Thermal treatment (°C)	A_2 (1–f)	B_2 (f)	t_{12} (μs)	t_2 (μs)	γ_2 ($s^{-1/2}$)	τ_2 (μs)	R^2
Time constants of luminescence kinetic processes (574 nm) (experimental)							
60	–	–	–	–		–	
500	3611	–	–	816.6	17.73	526	0.9994
600	3923	1099	2.93	836.3	9.52	660	0.9997
800	17,626 (0.71)	6700 (*0.29*)	2.21	848.4	10.89	647	0.9998
1000	110,183 (*0.69*)	46,526 (*0.31*)	2.11	634.7	1.97	616	0.9998
1200	250,776 (*0.70*)	98,576 (*0.30*)	3.02	671	0	671	0.9995

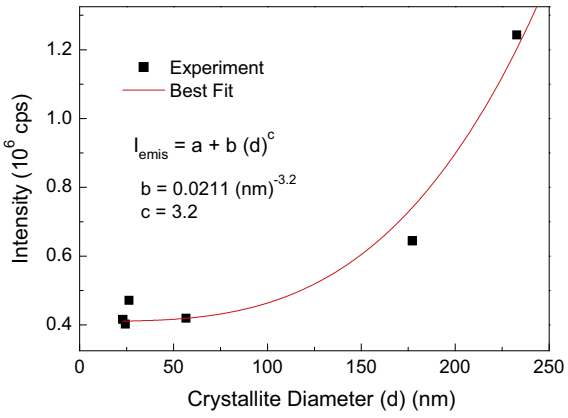

Fig. 8. Emission intensity (integrated between 560 and 650 nm) as a function of the mean crystallite size (diameter in nm), which was obtained by X-ray diffraction method, for the thermally treated nanopowder. Experimental values are represented by solid squares and best fit is given by solid line.

5. Conclusions

The nanocrystalline hydroxyapatites pure and doped with Eu^{3+} were successfully obtained. The luminescence results showed a red emission for as-synthesized samples with two mean broad emission bands at 592 nm and 616 nm, and a weak one at 579 nm. The thermal treatment (from 500 °C until 800 °C) induces the diffusion of europium ion, which was 100% located at Ca^{2+} (I) site in the as-synthesized samples, to Ca^{2+} (II) site. Site II seems to be more energetically stable to Eu^{3+}.

At 800 °C, the new re-arrangement of Eu^{3+} in hydroxyapatite lattice is 30% at site I and 70% at site II, and with the temperature increasing until 1200 °C no variation was observed on those europium ions distribution, showing that at 800 °C the europium diffusion process is over. However, the temperature increasing leads to an enhancement of the europium emission intensity, which reaches the maximum fluorescence intensity at 1200 °C.

Besides the strong increasing of the europium emission intensity observed for heated samples, the mean lifetimes of $^5D_0$ excited state of Eu^{3+} (site II), which is the dominant emission from europium in Eu:HAp increased from 526 μs (T = 500 °C) to 671 μs after the thermal treatment at T = 1200 °C, that indicates a luminescence efficiency augmentation of 22%.

On the other hand, the mean lifetimes of $^5D_0$ excited state of Eu^{3+} (site I) decreased from ~550 μs ($T \leqslant 800$ °C) to 300 μs (1200 °C), while exhibiting a short decay component of ~3 μs (590 nm), which is consistent with the short risetime observed for the 574 nm luminescence transient of Eu^{3+} (site II), both due to Eu^{3+} (site I) → Eu^{3+} (site II) energy transfer process.

The strong luminescence intensity observed for the sample thermally treated at T = 1200 °C should not be due to the luminescence efficiency of $^5D_0$ excited level improvement that increases only by 22%. But mostly due to the increase of the absorption at 394 or 460 nm by Eu^{3+} ion as the crystallite size growths with the thermal treatment at higher temperatures – absorption depends on the crystallite volume.

The complete analysis of the luminescence properties of the Eu^{3+} in HAp performed in this work, based on the results of the time-resolved luminescence spectroscopy applied to the synthesized and to the thermally treated samples constitutes the novelty itself, which details are given as following:

1- The Eu^{3+} ion distribution is non-random in HAp during the fast nanocrystal growth process at lower temperature (60 °C) by co-precipitation method (pH = 10), since 100% of Eu^{3+} ion substitutes Ca^{2+} at Ca^{2+} (I) site.
2- Thermal treatments at T > 500 °C allows Eu^{3+} ions to migrate from site I to site II, propitiated by the Ca^{2+} – vacancy – Eu^{3+} (charge compensator) diffusion through the HAp lattice.
3- A new distribution of Eu^{3+} ions is observed for samples thermal treated at $T \geqslant 800$ °C, where Eu^{3+} occupation changes to 70% at site II and 30% at site I. In this case, an Eu^{3+} (site I) → Eu^{3+} (site II) energy transfer can be measured and the decay of $^5D_0$ excited state of Eu^{3+} (site I) becomes very fast with a lifetime of ~3 μs. As a consequence, the emission spectrum of $^5D_0$ level is drastically modified by the strongest Eu^{3+} (site II) emission.
4- The integrated emission intensity of Eu^{3+} (I and II) (560–650 nm) drastically increases with the thermal treatment temperature more due to the crystallite size growth (d^3) than due to the augment of the luminescence efficiency that was estimated to increase only 22%.

Acknowledgements

The authors thank financial support from CNPq (480892/2013-0).

References

[1] H. Zheng, D. Gao, X. Zhang, E. He, J. Appl. Phys. 104 (1) (2008) 013506.
[2] Z. Chen, H. Chen, H. HU, M. Yu, F. Li, Q. Zhang, Z. Zhou, T. Yi, C. Huang, J. Am. Chem. Soc. 130 (10) (2008) 3023.
[3] J. Zhou, F. Li, Chem. Soc. Ver. 41 (2012) 1323.
[4] S.V. Dorozhkin, Calcium Orthophosphates in Nature, Biol. Med., Mater. 2 (2009) 399.
[5] S.J. Kalita, A. Bhardwaj, H.A. Bhatt, Mater. Sci. Eng. C 27 (2007) 441.
[6] F. Chen, P. Huang, Y. Zhu, J. Wu, C. Zhang, D. Cui, Biomaterials 32 (2011) 9031.
[7] P. Yang, Z. Quan, C. Li, X. Kang, H. Lian, Jun Lin, Biomaterials 29 (2008) 4341.
[8] R. Jagannathan, M. Kottaisamy, J. Phys.. Condensed Matter. 7 (1995) 845343466.
[9] M. Gaft, R. Reisfeld, G. Panczer, S. Shovala, B. Champagnon, G. Boulon, J. Lumin. 72–74 (1997) 572.
[10] A. Doat, F. Pelle, N. Gardant, A. Lebugle, J. Solid State Chem. 177 (2004) 1179.
[11] A. Zounani, D. Zambon, J.C. Cousseins, J. Alloys Compd. 82 (6) (1992) 188.
[12] R. Ternane, M. Trabelsi-Ayedi, N. Kbir-Ariguib, B. Piriou, J. Lumin. 81 (1999) 165.
[13] O.A. Graeve, R. Kanakala, A. Madadi, B.C. Williams, K.C. Glass, Biomaterials 31 (2010) 4259.
[14] M. Karbowiak, S. Hubert, J. Alloys Compd. 302 (2000) 87.
[15] E.V. Zubar, N.P. Efryushina, V.P. Dotsenko, Proceedings of the International Conference of Nanomaterials: Applications and Properties 2 (4) (2013) 04NABM09.
[16] C.S. Ciobanu, F. Massuyeau, E. Andronescu, M.S. Stan, A. Dinischiotu, D. Predoi, Digest J. Nanomater. Biostruct. 6 (4) (2011) 1639.
[17] N. Lakshminarasimhan, U.V. Varadaraju, J. Solid State Chem. 177 (2004) 3536.
[18] B. Piriou, D. Fahmi, J. Dexpert-Ghys, A. Taitai, J.L. Lacout, J. Lumin. 39 (1987) 97.
[19] L.D. da Vila, L. Gomes, L.V.G. Tarelho, S.J.L. Ribeiro, Y. Messaddeq, J. Appl. Phys. 93 (2003) 3873.
[20] A.I. Burshtein, JETP Lett. 35 (1972) 885.
[21] A.F.H. Librantz, L. Gomes, J. Lumin. 129 (2009) 376.
[22] L. Gomes, M. Oermann, H. Ebendorff-Heidepriem, D. Ottaway, T. Monro, S.D. Jackson, J. Appl. Phys. 110 (2011) 083111.
[23] L. Gomes, S.D. Jackson, J. Opt. Soc. Am. B 30 (6) (2013) 1410.
[24] L. Gomes, J. Lousteau, D. Milanese, E. Mura, S.D. Jackson, J. Opt. Soc. Am. B 31 (3) (2014) 429.
[25] D. Laurencin, N. Almora-Barrios, N.H. Leeuw, et al., Biomaterials 32 (2011) 1826.
[26] A. Doat, M. Fanjul, F. Pellé, et al., Biomaterials 24 (2003) 3365.
[27] L. Grigorjeva, D. Millers, K. Smits, et al., IOP Conf. Series: Materials Science and Engineering (2013) 49 012005.
[28] C. Yang, P. Yang, W. Wang, et al., J. Colloid Interf. Sci. 328 (2008) 203.
[29] M. Long, F. Hong, W. Li, et al., J. Lumin. 128 (2008) 428.
[30] P. Martin, G. Carlot, A. Chevarier, C. Den-Auwer, G. Panczer, J. Nucl. Mater. 275 (1999) 268.
[31] Z. Wei, L. Sun, C. Liao, J. Yin, X. Jiang, C. Yan, J. Phys. Chem. B 106 (2002) 10610.
[32] G.S. Ofelt, J. Chem. Phys. 37 (1962) 511.
[33] R. Reisfeld, Rare Earths Struct. Bonding 13 (1973) 53.
[34] H.-Q. Liu et al., J Alloys Compd. 448 (2008) 336–339.